SCIENCE CHINA Materials ARTICLES

mater.scichina.com link.springer.com

Published online 18 November 2019 | https://doi.org/10.1007/s40843-019-1212-x
Sci China Mater 2020, 63(3): 421–428

Iron-doping induced multiferroic in two-dimensional In_2Se_3

Huai Yang[1], Longfei Pan[1], Mengqi Xiao[1], Jingzhi Fang[1], Yu Cui[1] and Zhongming Wei[1,2*]

ABSTRACT **Multiferroic materials exhibit tremendous potentials in novel magnetoelectric devices such as high-density non-volatile storage. Herein, we report the coexistence of ferroelectricity and ferromagnetism in two-dimensional Fe-doped In_2Se_3 ($Fe_{0.16}In_{1.84}Se_3$, FIS). The Fe atoms were doped at the In atom sites and the Fe content is ~3.22% according to the experiments. Our first-principles calculation based on the density-functional theory predicts a magnetic moment of 5 μ_B per Fe atom when Fe substitutes In sites in In_2Se_3. The theoretical prediction was further confirmed experimentally by magnetic measurement. The results indicate that pure In_2Se_3 is diamagnetic, whereas FIS exhibits ferromagnetic behavior with a parallel anisotropy at 2 K and a Curie temperature of ~8 K. Furthermore, the sample maintains stable room-temperature ferroelectricity in piezoresponse force microscopy (PFM) measurement after the introduction of Fe atom into the ferroelectric In_2Se_3 nanoflakes. The findings indicate that the layered $Fe_{0.16}In_{1.84}Se_3$ materials have potential in future nanoelectronic, magnetic, and optoelectronic applications.**

Keywords: 2D materials, multiferroic, iron-doping, In_2Se_3

INTRODUCTION

Multiferroic materials refer to the materials exhibiting two or more primary ferroic properties (ferroelectric, ferromagnetic, and ferroelastic) simultaneously [1]. The multiferroics provide potential applications in the non-volatile storage devices controlled by an external electric/magnetic field [2,3]. However, the future integration technologies require quite smaller device size, especially the size of graphene and black phosphorus-based transistors or memories being reduced to the monolayer scale (<1 nm) [4,5]. A series of conventional three-dimensional (3D) materials, such as $BiFeO_3$, have been studied for many years [6]. However, due to the dangling bonds and leakage current originating from quantum tunneling, the nano-devices based on traditional 3D materials show poor performance [7]. Since the first 2D ferroelectric material SnTe was discovered in 2016, which holds a low Curie temperature (T_C) below room temperature and is hard to be used in practical applications [8], researchers have discovered that the van der Waals materials $CuInP_2S_6$ and In_2Se_3 also exhibit 2D ferroelectricity at room temperature [9–12]. Especially for In_2Se_3, it is reported that it still maintains its ferroelectricity and piezoelectricity even down to monolayer [13]. Its excellent sustainability and performance prompt people to use it in ferroelectric applications such as non-volatile memristor [14]. Furthermore, the coexistence of out-of-plane and in-plane piezoelectricity in In_2Se_3 makes it promising in energy harvesting system and self-power nanodevice responding to strain from all directions [15]. While for 2D materials, it is very difficult to realize ferroelectricity and ferromagnetism simultaneously especially down to nanometers [11].

Recently, 2D ferromagnetic materials have been receiving tremendous attention and intensively researched in recent years [16]. The 2D magnetic $Cr_2Ge_2Te_6$, CrI_3 and Fe_3GeTe_2 have been reported to have novel properties such as layer-dependent ferromagnetic and adjustable Curie temperature [17–19]. Except exploring rarely intrinsic 2D ferromagnetic materials which are hard to be stable for monolayer, several existing methods such as defect engineering *via* vacancies, doping atoms, grain boundaries or edges, and introducing magnetic species *via* intercalation or substitution could also facilitate stable ferromagneticity [17]. The dilute ferromagnetic semiconductors, prepared by substituting magnetic ions into nonmagnetic semiconductors, have recently attracted great interest due to the potential to create new classes of

[1] State Key Laboratory of Superlattices and Microstructures, Institute of Semiconductors, Chinese Academy of Sciences & Center of Materials Science and Optoelectronics Engineering, University of Chinese Academy of Sciences, Beijing 100083, China
[2] Beijing Academy of Quantum Information Sciences, Beijing 100193, China
* Corresponding author (email: zmwei@semi.ac.cn)

spin-dependent electronic devices [20]. Besides, doping magnetic atoms into 2D material has been realized in Co-doped MoS_2, Fe-doped SnS_2 in our previous work [21,22]. Doping ferromagnetic atoms such as Fe, Co and Mn into ferroelectric materials such as $BaTiO_3$ and $SrTiO_3$ has been realized to achieve room-temperature multiferroic [23–25]. Furthermore, some research groups proposed multiferroic materials by doping or modifying some monolayers, such as black phosphorus and graphene [26]. It is reported that 2D $CuCrP_2S_6$ exhibits multiferroic proved by experiment and theory [11]. All of these discoveries attracted great interests in exploring more multiferroic materials.

In this work, we combine ferroelectric and ferromagnetic *via* doping magnetic atom Fe into 2D ferroelectric crystals In_2Se_3. The Fe-doped In_2Se_3 ($Fe_{0.16}In_{1.84}Se_3$, FIS) nanoflakes were obtained *via* mechanical exfoliation. The piezoresponse force microscopy (PFM) measurement shows the FIS flakes exhibit ferroelectric properties even down to several nanometer. By applying opposite electric field between the thin-layer FIS, the polarization of domain can be inversed. Magnetic measurements show that FIS possesses ferromagnetic behavior with a perpendicular anisotropy at 2 K and a T_C of ~8 K. The 2D multiferroic FIS materials have great potentials to apply in electromagnetism interaction and realize electric controlling magnetic. The realization of multiferroic provides great opportunities to explore new multiferroic material with higher T_C and excellent properties.

EXPERIMENTAL SECTION

Bulk crystal growth and sample preparation

High-quality single crystals of FIS were obtained by the chemical vapor transport technique using iodine as a transport agent. Powder of high purity In (99.99%), Se (99.99%) and $FeCl_3$ (99.99%) were weighed in stoichiometric proportions and placed in an quartz ampoule. The mixture was placed along with 2 mg cm^{-3} of iodine (99.99%) ball. Then the ampoule was evacuated of air and brought to 10^{-5} Torr before sealing. The growth was conducted in a horizontal two-zone tube furnace with the temperature gradient setting at 800/950°C [27], and the system was heated up to 700/800°C for chemical combination for 3 days and 800/950°C for growth crystal for 10 days. The system was finally cooled down to room temperature at a 10°C/h rate. To be specific, the Fe-In_2Se_3 crystals were obtained as hexagon-shaped crystals several centimeters long concentrated in the bottle of the quartz tube. The desired Fe-In_2Se_3 crystals could be easily picked out with tweezers by its appearance and the position of crystal in quartz tube.

Composition and characteristics

X-ray photoelectron spectroscopy (XPS) was conducted using Thermo escalab 250Xi. Scanning transmission electron microscopy (STEM) was performed using FEI Titan 80-300. The atomic force microscopy (AFM) and PFM measurements were performed by Bruker Dimension Icon with tapping mode. The PFM measurements were performed with Pt/Ir conducting tips with 75 kHz excitation frequency under ambient condition. Gold coated heavily doped silicon was used as the conductive substrates. Magnetic measurements were performed by using a Quantum Design MPMS3 Superconducting Quantum Interference Device (SQUID).

Theoretical calculation and simulations

Electronic structure calculations were carried out using the projector augmented wave (PAW) method and planewave basis set as implemented in the Vienna *Ab Initio* Simulation Package (VASP) [28,29]. The generalized gradient approximation and Perdew–Burke–Ernzerhof functional (GGA-PBE) formalism of exchange and correlation functional [30,31] were employed throughout electronic-structure calculations. For more accurate calculation of optical property, hybrid functional (HSE06) was used [32,33], in which the hybrid functional was mixed with 25% exact Hartree–Fock (HF) exchange. A kinetic energy cutoff of 450 eV and a Gamma k–mesh of 7×7×1 sampling in the full Brillouin zone were used in our calculations. When calculating optical properties, a Gamma k–mesh of 9×9×1 sampling in the full Brillouin zone was used in our calculations. The U parameter is a coefficient in Hubbard correction. The Hubbard correction term is defined as follows [34]:

$$E_U = \frac{U}{2}\sum_{\sigma}\left[\left(\sum_{m_1} n^{\sigma}_{m_1,m_1}\right) - \left(\sum_{m_1,m_2} n^{\sigma}_{m_1,m_2} n^{\sigma}_{m_2,m_1}\right)\right], \quad (1)$$

where σ represents the spin states, and m_1 and m_2 represent the projections of the orbital momentum (m_1, m_2=−2, −1, 0, 1, 2 in the case of d electrons). We also used the GGA+U method in calculations for the electronic structure of Fe-doped In_2Se_3. The supercell size was 2×2×1 and the doping concentration was about 3.45% when Fe substitutes In sites in In_2Se_3. The simulations in our article were performed at 0 K. To obtain the appropriate U value, we performed a calculation using a self-consistent method [35] with Quantum-ESPRESSO (QE) [36]. The real space grid techniques were used with an

energy cutoff of more than 100 Hartree as a required cutoff energy in numerical integration. The geometries were optimized until all residual forces on each atom were smaller than 0.01 eV $Å^{-1}$. In all of our calculations in this paper, van der Waals forces were considered through dispersion-corrected density functional theory (DFT-D2) [37].

RESULTS AND DISCUSSION

Group III-VI compound In_2Se_3 is a 2D layered semiconductor with a bandgap of 1.3 eV [38]. For an individual In_2Se_3 layer, five triangular atomic lattices in the sequence of Se–In–Se–In–Se lattices are connected with covalent bonds costructing the In_2Se_3 quintuple layer (QL). The simulated doping structure is shown in Fig. 1a. While for the bulk crystal belonging to *R*3*m* or *P*63/*mmc* space group, the In_2Se_3 layers are stacked by van der Waals force [9]. The crystal structure is formed by 2D In_2Se_3 QLs, which are stacked *via* weak van der Waals interactions. The polarization of ferroelectricity originates from the asymmetric position of the Se atom in the middle, which spontaneously breaks the centrosymmetry [39]. In the out-of-plane direction, the significant difference in layer spacing between the intermediate Se layer and the two In layers results in a net electric dipole [13].

The XPS was carried out to determine the concentration and chemical states of Fe element. By referencing the C 1s peak to 284.7 eV, the binding energy values were corrected and Fig. 1b shows the XPS spectra of FIS. According to previous literature, the binding energies of Fe $2p_{3/2}$ in Fe_2O_3, $FeCl_3$, and $FeCl_2$ are 710, 711.5, and 710.6 eV, respectively [40]. The binding energy of Fe $2p_{3/2}$ electron peak locates at ~711.3 eV, which is close to the binding energy of Fe(III) valence for $FeCl_3$. This excludes the formation of iron metal clusters since the binding energy of Fe $2p_{3/2}$ for iron metal is 707 eV, demonstrating that the Fe atoms tend to substitute In atoms instead of Se atoms [21]. The In_2Se_3 nanosheet can be mechanically exfoliated on SiO_2/Si substrate or Cu grid by putting the crystal on Scotch tape and further sticking on the substrate. The energy-dispersive X-ray spectroscopy (EDS) of the nanosheet (Fig. 1c) shows that it contains In, Se and Fe elements and the concentration of Fe is ~3.22%. Thus, the formula of the obtained Fe-doped In_2Se_3 is $Fe_{0.16}In_{1.84}Se_3$. Furthermore, the EDS mapping was performed to characterize the distribution of In, Se and Fe in nanosheet as shown in Fig. 1d. The corresponding elemental mapping images of In, Se and Fe in a selected

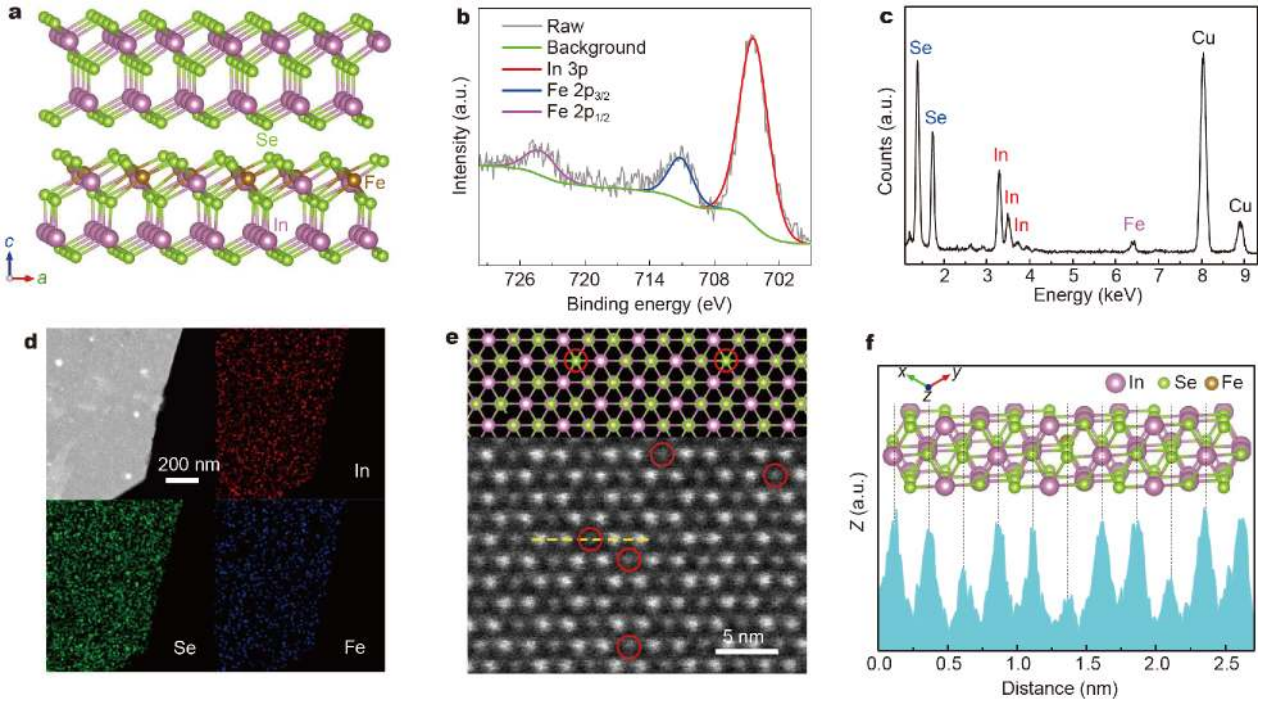

Figure 1 (a) Crystal structure of bulk FIS. (b) XPS of different Fe doped In_2Se_3. (c) EDS of the Fe doped In_2Se_3 flake. (d) EDS elemental mapping images of In, Se and Fe, respectively. (e) High-resolution STEM image of the FIS flake; the red circles are Fe atoms. (f) *Z*-contrast mapping in the areas around red circles in (e).

region of a typical crystal indicate that the In, Se and Fe elements are homogeneously distributed throughout the entire flake, demonstrating that the Fe atom can be uniformly doped into the crystal.

In order to investigate the crystal structure and chemical composition of the as-exfoliated FIS, high-angle annular dark-field scanning transmission electron microscopy (HAADF-STEM) was further performed. The low-resolution TEM image in Fig. 1d shows a part of the few-layer FIS flake on the holey carbon TEM grid. The STEM image reveals that the crystal agrees with the hexagonal structure and *P*63/*mmc* symmetry as shown in Fig. 1e. Using a high-resolution STEM image, the In, Fe and Se atoms were directly distinguished according to the difference of the *Z*-contrast intensity distribution as shown in Fig. 1f. Fe atoms were doped at the In atom sites. The In–Se distance is 0.236 nm, which agrees well with the theoretical value of 0.233 nm. Considering STEM, EDS, and XPS results together, we believe that Fe element incorporates into the lattice frame of In_2Se_3 by substituting the position of indium atoms.

To verify the ferroelectricity and investigate the spontaneous polarization originating from the broken inversion symmetry and polar structure of FIS, we carried out PFM measurement by exfoliating the FIS crystals on conductive Pt/Si substrates (Si substrate with a 30 nm Pt metal top layer). By measuring minute expansion and contraction of the sample under an applied electric field, PFM can monitor and acquire the information of amplitude (magnitude of response) and phase (polarization direction) of the cantilever deflection. In order to minimize the electrostatic effect, the electrostatic gun was targeted to the sample and the stiff cantilever with a high spring constant was adopted while using pulsed DC mode in measurement. The AFM image and corresponding out-of-plane PFM phase image are shown in Fig. 2a, b. As can be seen, the phase image reveals two out-of-plane polarization directions with opposite phase contrasts in FIS flake, which displays no obvious connection with the thickness of samples inferred form the AFM contrast, demonstrating that PFM phase contrast stems from spontaneous polarization instead of height difference [9]. The deep and shallow regions have a phase difference of 180°, which corresponds to ferroelectric domains with upward and downward polarization vectors perpendicular to the horizontal plane, respectively. The polarization of ferroelectric domains can be manipulated by applying the electric field between the nanoflakes. By applying opposite voltage (−5 and +6 V) on the tip to scan the sample, the polarization direction can be in-

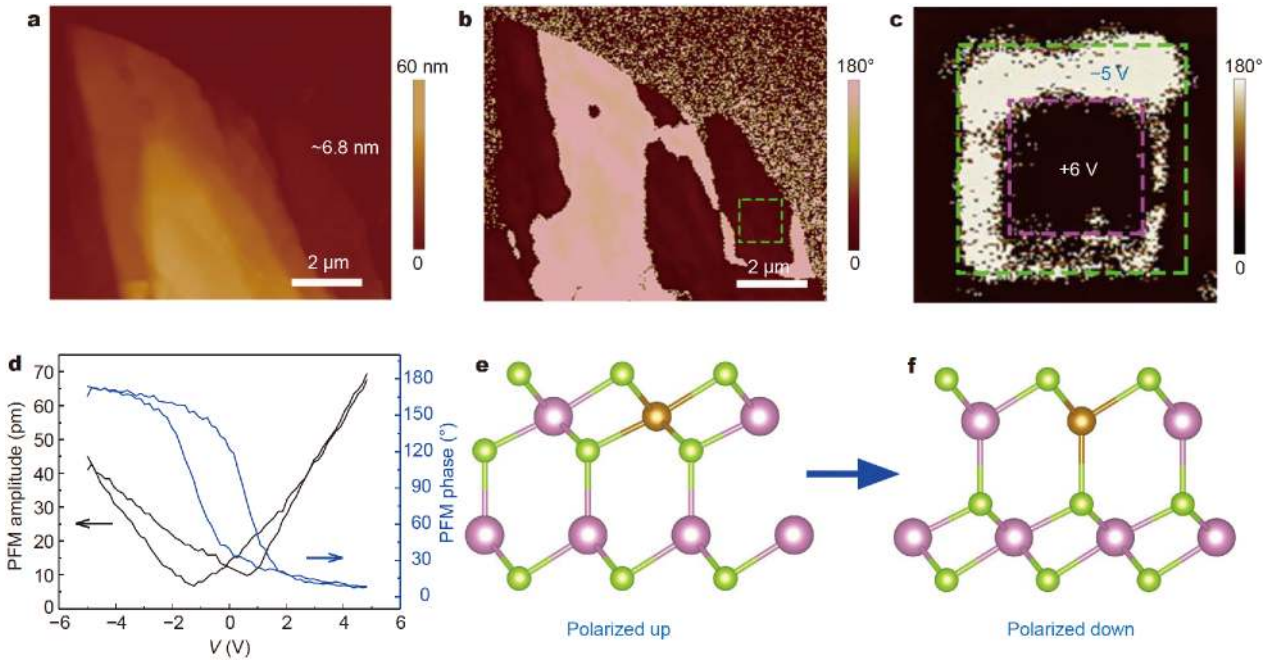

Figure 2 PFM investigation of the as-grown FIS on Pt/Si substrate. (a) AFM image of typical thin flakes with different thicknesses. (b) The corresponding PFM images of phase. (c) Out-of-plane phase image of a 6.8 nm thick In_2Se_3 flake acquired immediately after writing two square patterns by applying −5 and +6 V voltages consecutively. (d) PFM amplitude and PFM phase hysteresis loops on a 20 nm thick flake indicating polarization reversal under an external electrical field. Schematic model of the single quintuple layer after polarized up (e) and polarized down (f).

versed. The larger square was first applied with −5 V, and then the middle square strip was applied with +6 V. After the sample was scanned for half an hour constantly, the domain pattern maintained obvious phase contrast. The write-read patterns demonstrate the nonvolatile properties of the ferroelectric domains [10]. To further investigate the ferroelectric hysteresis behavior of FIS nanosheet, we applied electric field on the top of material using a conductive Pt/Ir tip. The applied electric field between conductive tip and Pt/Si substrate is able to manipulate the polarization direction of the middle sample. The obtained butterfly like loops and hysteresis loops are presented in Fig. 2d. It indicates that the imposed DC voltage in the tip of ± 5 V is enough to reverse the polarization of ferroelectric domains to the opposite orientation. The butterfly like voltage dependent amplitude loop exhibits an amplitude change about 34 pm, corresponding to the phase switching 180°. The asymmetry of amplitude loop contributes to the leakage of high concentration of free carrier. The inversion and hysteresis of the both curves indicate the ferrelectric polarization orientation can be controlled by applied electric field artificially. Fig. 2e, f show the schematic model of the single quintuple layer after polarized up and polarized down. The PFM test demonstrates that even after bringing Fe atom into the structure of ferroelectric In_2Se_3, the FIS sample maintains stable room-temperature ferroelectricity [41].

The magnetization measurements of pure In_2Se_3 and FIS single-crystal flake with a diameter of ~7 mm and a thickness of ~2 μm were carried out using the SQUID. As indicated in Fig. 3a, the pure In_2Se_3 is diamagnetic at 2 K both in the $H_\perp$ nd $H_{||}$ directions because of the saturated electronic structure. Fig. 3b shows the observed magnetization vertical to the basal plane as a function of the temperature. The zero field cooling curve indicates the T_C is ~8 K. By adjusting the temperature and magnetic field, the magnetization (M) *versus* magnetic field (H) in the range of −6 to 6 kOe were measured for the FIS sample at 2 and 300 K, respectively. The magnetic field with two different magnetic directions was respectively applied in perpendicular to the sheet ($H_\perp$) and parallel to the sheet ($H_{||}$). It indicates that the magnetization parallel to the basal plane is much higher than that measured perpendicular to the basal plane. The M-H curve of the FIS sheet shows obvious anisotropy in the $H_{||}$ and $H_\perp$ directions at

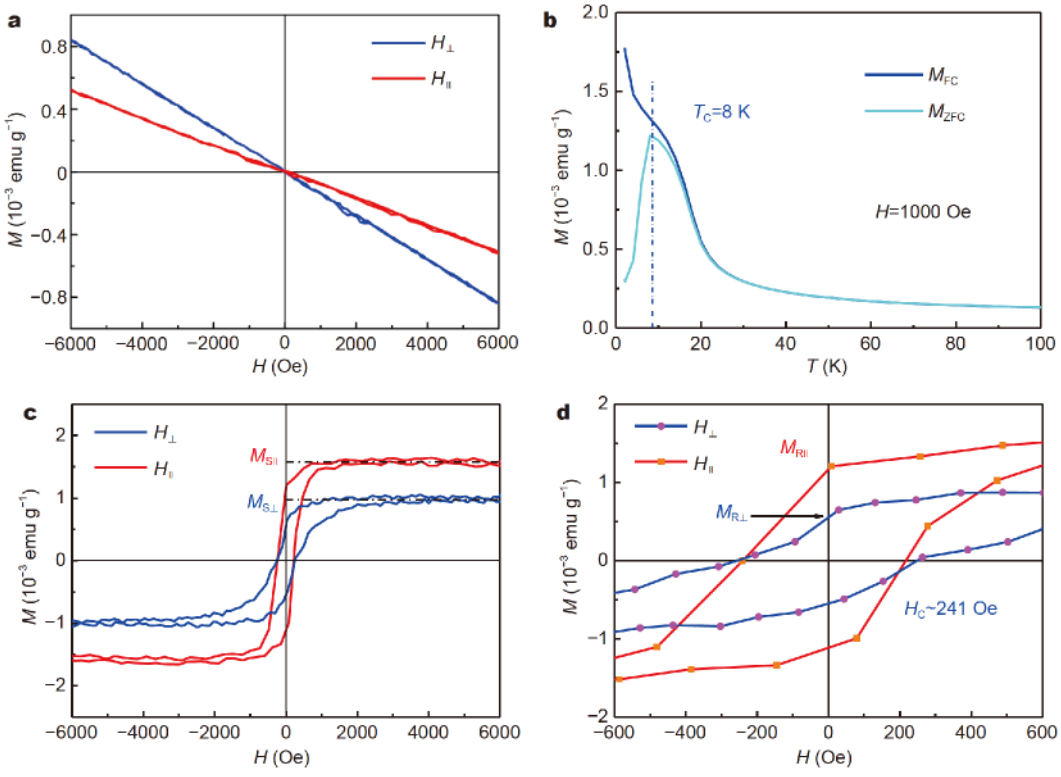

Figure 3 (a) Magnetic hysteresis loops at 2 K for In_2Se_3. (b) Magnetization as a function of temperature for FIS from 2 to 100 K. The applied magnetic field was 1000 Oe. (c) Magnetic hysteresis loops for FIS in parallel and perpendicular directions at 2 K. (d) Expanded view of the loop of FIS in (c).

2 K, respectively. The saturation magnetization (M_S) in the $H_\perp$ and $H_{||}$ directions for FIS is 9.77×10^{-4} and 1.57×10^{-3} emu g^{-1}, respectively. The remnant magnetization (M_R) in the $H_\perp$ and $H_{||}$ directions for FIS is 5.52×10^{-4} and 1.16×10^{-3} emu g^{-1}, respectively. The coercivity (H_c) and remnant magnetization of $H_\perp$ are 241 Oe, which is approximately same to those of $H_{||}$. To be mentioned, the doping concentration is very low (about 3.22%) and the size of the sample is small in the experiment. Thus, the magnetism of the sample in experiment is relatively week. We discuss the detailed origin of the magnetism and the magnetic anisotropy of the FIS sheet below. The magnetism of bulk Fe-doped In_2Se_3 was investigated by first-principles calculations. We calculated two different doping positions of Fe. We first calculated accurate Hubbard U value of Fe, using the self-consistent method [35]. The U values at the two doping positions are 3.56 and 3.24 eV, respectively. The band structure of Fe-doped In_2Se_3 at both doping positions was calculated by GGA+U method. The doping structure in Fig. 1a behaves as a semiconductor characteristic, which is consistent with the experimental results. Therefore, we only show the calculation results of Fe-doped In_2Se_3 with the doping position in Fig. 4. The total magnetic moment of the doped Fe atom calculated by the GGA+U method is 5 μ_B. The distribution of spin-polarized charge density is shown in Fig. 4a. The calculated and experimental absorption spectra parallel/perpendicular to c-axis are also shown in Fig. 4b. As can be seen, there is obvious difference in the absorption spectra from 200 to 800 nm between intrinsic In_2Se_3 and the Fe-doped In_2Se_3. In experiment, the absorption peaks have been red shifted in parallel direction after doping with the Fe atom, which is consistent with the theoretical calculation. The Se atoms bonded to the Fe dopant atom yield a magnetic moment of −0.003 μ_B, which has little effect on the total magnetic moment. Fig. 4e shows the crystal field splitting of the 3d electrons of the doped Fe atoms. Since the doped Fe is affected by the octahedral crystal field in In_2Se_3, the 3d electrons of the Fe atom are split into the t_{2g} states and the e_g states. And according to the projected band structure in Fig. 4c, f, the occupancy of the 3d electrons of Fe atoms in the ground state is demonstrated in Fig. 4d. The occupancy of the 3d electrons of Fe in the figure also indicates that the doped Fe atoms will have a magnetic moment of 5 μ_B, which is consistent with the calculations we men-

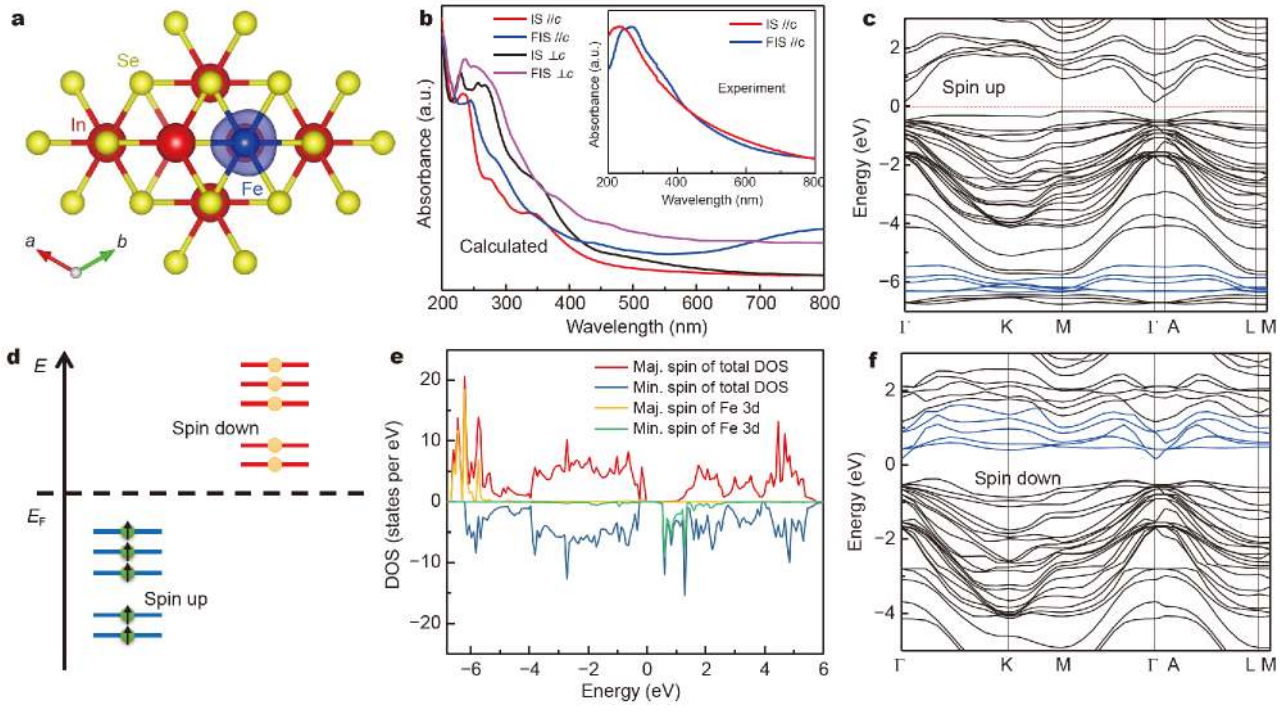

Figure 4 Theoretical calculations of the Fe–In_2Se_3 monolayer. (a) Atomic structure of the Fe–In_2Se_3 monolayer. Red, yellow, and blue balls represent In, Se, and Fe atoms, respectively. (b) Absorbance spectra of bulk Fe–In_2Se_3 crystal in calculation and experiment. Projected band structures of the Fe–In_2Se_3 monolayer for up-spin (c) and down-spin (f) channels, respectively. Blue lines denote the contribution of Fe atoms in the total band structure, respectively. The Fermi level was set to zero. (d) Schematic of the Fe 3d electron arrangement with spin in Fe–In_2Se_3. (e) Total density of states of the Fe–In_2Se_3 monolayer.

tioned earlier. As shown in Fig. 4d, the spin polarization of the material is mainly derived from the 3d of the Fe-doped In_2Se_3 with second electrons of the Fe atoms.

The projected density of states shows that the majority spin states of Fe 3d electrons are all in the valence band. Meanwhile, the minority spin states of Fe 3d electrons are all in the conduction band. This is also consistent with the projected band structure in Fig. 4c, f. To study the preferred magnetic coupling, the energies of the ferromagnetism and antiferrromagnetism states of the (2×2×1) supercell for the Fe-doped In_2Se_3 were calculated. The formation energy of ferromagnetism is −248.178 eV and the formation of antiferrromagnetism is −247.895 eV. Thus, the exchange energy E_{ex} (E_{ex}=E_{AntiFM}−E_{FM}. FM and AntiFM stands for ferromagnetism and antiferromagnetism, respectively) is 0.283 eV and the total magnetic moment is 5 μ_B. A positive exchange energy indicates that the ground state of the system is FM. It is found that FM coupling exists in 2D Fe-doped In_2Se_3 with E_{ex} = 283 meV per (2×2×1) supercell.

CONCLUSIONS

In summary, we have successfully synthesized a 2D multiferroic FIS crystal which exhibits ferroelectricity and ferromagnetism simultaneously. The PFM measurement indicates the FIS flake exhibits ferroelectric properties even down to several nanometer. The magnetic measurements indicate that pure In_2Se_3 is diamagnetic, whereas FIS exhibits ferromagnetic behavior with a parallel anisotropy at 2 K and a T_C of ~8 K. The first-principles calculation based on the DFT confirms the ferromagnetism and predicted a magnetic moment of 5 μ_B per Fe atom when Fe substitutes In sites in In_2Se_3. The findings suggest that the layered FIS has potential in future nanoelectronic, magnetic, and optoelectronic applications. The realization of multiferroic provides great opportunities to explore novel multiferroic materials with higher T_C and excellent performance.

Received 14 August 2019; accepted 22 October 2019; published online 18 November 2019

1 Eerenstein W, Mathur ND, Scott JF. Multiferroic and magnetoelectric materials. Nature, 2006, 442: 759–765
2 Seixas L, Rodin AS, Carvalho A, *et al.* Multiferroic two-dimensional materials. Phys Rev Lett, 2016, 116: 206803
3 Bibes M. Nanoferronics is a winning combination. Nat Mater, 2012, 11: 354–357
4 Radisavljevic B, Radenovic A, Brivio J, *et al.* Single-layer MoS_2 transistors. Nat Nanotech, 2011, 6: 147–150
5 Sangwan VK, Jariwala D, Kim IS, *et al.* Gate-tunable memristive phenomena mediated by grain boundaries in single-layer MoS_2. Nat Nanotech, 2015, 10: 403–406
6 Wang J, Neaton JB, Zheng H, *et al.* Epitaxial $BiFeO_3$ multiferroic thin film heterostructures. Science, 2003, 299: 1719–1722
7 Makhdoom AR, Akhtar MJ, Khan RTA, *et al.* Association of microstructure and electric heterogeneity in $BiFeO_3$. Mater Chem Phys, 2013, 143: 256–262
8 Chang K, Liu J, Lin H, *et al.* Discovery of robust in-plane ferroelectricity in atomic-thick SnTe. Science, 2016, 353: 274–278
9 Zhou Y, Wu D, Zhu Y, *et al.* Out-of-plane piezoelectricity and ferroelectricity in layered α-In_2Se_3 nanoflakes. Nano Lett, 2017, 17: 5508–5513
10 Cui C, Hu WJ, Yan X, *et al.* Intercorrelated in-plane and out-of-plane ferroelectricity in ultrathin two-dimensional layered semiconductor In_2Se_3. Nano Lett, 2018, 18: 1253–1258
11 Lai Y, Song Z, Wan Y, *et al.* Two-dimensional ferromagnetism and driven ferroelectricity in van der Waals $CuCrP_2S_6$. Nanoscale, 2019, 11: 5163–5170
12 Liu F, You L, Seyler KL, *et al.* Room-temperature ferroelectricity in $CuInP_2S_6$ ultrathin flakes. Nat Commun, 2016, 7: 12357
13 Ding W, Zhu J, Wang Z, *et al.* Prediction of intrinsic two-dimensional ferroelectrics in In_2Se_3 and other III_2-VI_3 van der Waals materials. Nat Commun, 2017, 8: 14956
14 Xue F, He X, Retamal JRD, *et al.* Gate-tunable and multidirection-switchable memristive phenomena in a van der Waals ferroelectric. Adv Mater, 2019, 31: 1901300
15 Xue F, Zhang J, Hu W, *et al.* Multidirection piezoelectricity in mono- and multilayered hexagonal α-In_2Se_3. ACS Nano, 2018, 12: 4976–4983
16 Gong C, Zhang X. Two-dimensional magnetic crystals and emergent heterostructure devices. Science, 2019, 363: eaav4450
17 Gong C, Li L, Li Z, *et al.* Discovery of intrinsic ferromagnetism in two-dimensional van der Waals crystals. Nature, 2017, 546: 265–269
18 Huang B, Clark G, Navarro-Moratalla E, *et al.* Layer-dependent ferromagnetism in a van der Waals crystal down to the monolayer limit. Nature, 2017, 546: 270–273
19 Deng Y, Yu Y, Song Y, *et al.* Gate-tunable room-temperature ferromagnetism in two-dimensional Fe_3GeTe_2. Nature, 2018, 563: 94–99
20 Chen L, Yang X, Yang F, *et al.* Enhancing the Curie temperature of ferromagnetic semiconductor (Ga,Mn)As to 200 K *via* nanostructure engineering. Nano Lett, 2011, 11: 2584–2589
21 Li B, Xing T, Zhong M, *et al.* A two-dimensional Fe-doped SnS_2 magnetic semiconductor. Nat Commun, 2017, 8: 1958
22 Li B, Huang L, Zhong M, *et al.* Synthesis and transport properties of large-scale alloy $Co_{0.16}Mo_{0.84}S_2$ bilayer nanosheets. ACS Nano, 2015, 9: 1257–1262
23 Venkata Ramana E, Yang SM, Jung R, *et al.* Ferroelectric and magnetic properties of Fe-doped $BaTiO_3$ thin films grown by the pulsed laser deposition. J Appl Phys, 2013, 113: 187219
24 He J, Lu X, Zhu W, *et al.* Induction and control of room-temperature ferromagnetism in dilute Fe-doped $SrTiO_3$ ceramics. Appl Phys Lett, 2015, 107: 012409
25 Yao D, Zhou X, Ge S. Raman scattering and room temperature ferromagnetism in Co-doped $SrTiO_3$ particles. Appl Surf Sci, 2011, 257: 9233–9236
26 Hu T, Kan E. Progress and prospects in low-dimensional multiferroic materials. WIREs Comput Mol Sci, 2019, 9: e1409
27 Ho CH, Lin MH, Pan CC. Optical-memory switching and oxygen detection based on the CVT grown γ- and α-phase In_2Se_3. Sens Actuat B-Chem, 2015, 209: 811–819

28 Kresse G, Furthmüller J. Efficient iterative schemes for *ab initio* total-energy calculations using a plane-wave basis set. Phys Rev B, 1996, 54: 11169–11186
29 Kresse G, Furthmüller J. Efficiency of *ab-initio* total energy calculations for metals and semiconductors using a plane-wave basis set. Comput Mater Sci, 1996, 6: 15–50
30 Zhang Y, Yang W. Comment on "Generalized gradient approximation made simple". Phys Rev Lett, 1998, 80: 890
31 Perdew JP, Burke K, Ernzerhof M. Generalized gradient approximation made simple. Phys Rev Lett, 1996, 77: 3865–3868
32 Heyd J, Scuseria GE, Ernzerhof M. Hybrid functionals based on a screened Coulomb potential. J Chem Phys, 2003, 118: 8207–8215
33 Paier J, Marsman M, Hummer K, *et al.* Screened hybrid density functionals applied to solids. J Chem Phys, 2006, 124: 154709
34 Dudarev SL, Botton GA, Savrasov SY, *et al.* Electron-energy-loss spectra and the structural stability of nickel oxide: An LSDA+U study. Phys Rev B, 1998, 57: 1505–1509
35 Kulik HJ, Cococcioni M, Scherlis DA, *et al.* Density functional theory in transition-metal chemistry: a self-consistent Hubbard-U Approach. Phys Rev Lett, 2006, 97: 103001
36 Giannozzi P, Baroni S, Bonini N, *et al.* QUANTUM ESPRESSO: a modular and open-source software project for quantum simulations of materials. J Phys-Condens Matter, 2009, 21: 395502
37 Grimme S. Accurate description of van der Waals complexes by density functional theory including empirical corrections. J Comput Chem, 2004, 25: 1463–1473
38 Zhou J, Zeng Q, Lv D, *et al.* Controlled synthesis of high-quality monolayered α-In_2Se_3 *via* physical vapor deposition. Nano Lett, 2015, 15: 6400–6405
39 Xiao J, Zhu H, Wang Y, *et al.* Intrinsic two-dimensional ferroelectricity with dipole locking. Phys Rev Lett, 2018, 120: 227601
40 Grosvenor AP, Kobe BA, Biesinger MC, *et al.* Investigation of multiplet splitting of Fe 2p XPS spectra and bonding in iron compounds. Surf Interface Anal, 2004, 36: 1564–1574
41 Qiu S, Li W, Liu Y, *et al.* Phase evolution and room temperature ferroelectric and magnetic properties of Fe-doped $BaTiO_3$ ceramics. Trans Nonferrous Met Soc China, 2010, 20: 1911–1915

Acknowledgements This work was financially supported by the National Key Research and Development Program of China (2017YFA0207500), the National Natural Science Foundation of China (61622406, 61571415 and 51502283), the Strategic Priority Research Program of Chinese Academy of Sciences (XDB30000000), and Beijing Academy of Quantum Information Sciences (Y18G04).

Author contributions Yang H and Wei Z conceived the study. Yang H conducted most experiments and wrote the manuscript with support from Wei Z. Pan L performed the DFT calculations and wrote the theory part. Xiao M, Fang J and Cui Y provided experimental assistance and theoretical discussion. All authors contributed to the general discussion.

Conflict of interest The authors declare that they have no conflict of interest.

Huai Yang is currently a PhD candidate at the Institute of Semiconductors, Chinese Academy of Sciences, under the supervision of Prof. Zhongming Wei. His current research interests include the synthesis of low-dimensional materials and their related electronic, photoelectric, ferroelectric and ferromagnetic properties.

Zhongming Wei received his BSc degree from Wuhan University (China) in 2005, and PhD from the Institute of Chemistry, Chinese Academy of Sciences in 2010. From August 2010 to January 2015, he worked as a postdoctoral fellow and then Assistant Professor at the University of Copenhagen, Denmark. Currently, he is a professor at the Institute of Semiconductors, Chinese Academy of Sciences. His research interests include low-dimensional semiconductors and their functional devices.

铁掺杂诱导二维硒化铟的多铁性

杨淮[1], 潘龙飞[1], 肖梦琪[1], 房景治[1], 崔宇[1], 魏钟鸣[1,2*]

摘要 多铁材料具有巨大的潜力, 可应用于新型磁电设备, 如高密度非易失性存储等. 在本工作中, 我们报道了一种具有铁电性和铁磁性共存特性的新型二维铁掺杂硒化铟. 实验结果显示, Fe原子在In原子位点进行了替位掺杂, Fe的含量约为3.22%, 其化学式为$Fe_{0.16}In_{1.84}Se_3$. 基于密度泛函理论第一性原理计算预测, 当Fe替代硒化铟中In的位置时, 每个Fe原子的磁矩为5 μ_B. 我们通过量子干涉超导测试进一步证实了理论预测. 磁性测量表明纯硒化铟是抗磁性的, 而$Fe_{0.16}In_{1.84}Se_3$表现出铁磁行为, 在2 K时具有平行各向异性, 居里温度约为8 K. 此外, 压电力响应测试表明Fe原子掺杂进入铁电硒化铟纳米薄片后仍保持稳定的室温铁电性. 研究结果表明, 层状多铁材料$Fe_{0.16}In_{1.84}Se_3$在未来的纳米电子、磁性和光电器件中具有潜在的应用前景.

